Electrical Power and Energy Systems 131 (2021) 107087

Contents lists available at ScienceDirect

International Journal of Electrical Power and Energy Systems

journal homepage: www.elsevier.com/locate/ijepes

Voltage stability analysis of power systems with a large number of non-synchronous machine sources connected

Guoteng Wang, Zheng Xu *, Zheren Zhang

College of Electrical Engineering, Zhejiang University, Hangzhou 310027, Zhejiang Province, PR China

ARTICLE INFO

Keywords:
Line commutated converters
Voltage source converters
Voltage stability analysis

ABSTRACT

Compared with synchronous generators, the steady-state and dynamic characteristics of non-synchronous machine sources represented by line commutated converters (LCC) and voltage source converters (VSC) are quite different. The voltage stability of power systems will be changed when a large number of non-synchronous machine sources (NSMS) are connected. The voltage stability of power systems with NSMSs connected is analyzed in this paper. Firstly, based on the relationship between the Jacobian matrix singularity and the small disturbance voltage stability (SDVS), the impact of NSMSs on the SDVS of active systems is analyzed. Secondly, whether there is a reasonable voltage solution in the transient process is taken as a large-disturbance voltage stability (LDVS) criterion, the impact of NSMSs on the LDVS of active systems is studied. Thirdly, for a special scenario where the VSC supplies power to a passive system, the requirements of the voltage stability on load types and VSC parameters are discussed. Finally, based on the Power System Simulator/Engineering (PSS/E), simulations are carried out in the Shanghai power system and a passive power system, and the theoretical analysis results are verified.

1. Introduction

Non-synchronous machine sources (NSMS) can be divided into two types: grid forming converters and grid following converters. The grid forming converter is a voltage source converter (VSC) whose DC voltage must be kept constant. Typical representatives of the grid forming converter are VSCs with voltage amplitude and phase control or virtual synchronous machine control [1,2]. Typical representatives of the grid following converter are line-commutated converters (LCC) and VSCs with direct current control [3]. The target of the grid following converter is to control the amplitude and phase of the current injected into the power system. In China, the high voltage direct current (HVDC) transmission system based on LCCs is the main technical means of long-distance transmission [4]. The LCC has become a kind of high-proportion power sources in the load center of China. In some provinces of China, the import power through the LCC even exceeds 30% of the total load. The VSC is the main technical means for the delivery of renewable energy. As wind power and solar energy gradually replace fossil energy, the VSC will become the mainstream type of power sources for future power grids [5,6]. The grid forming VSC is mainly connected to weak AC systems or passive systems, while the grid following VSC is mainly connected to strong AC systems [7]. The large-scale feeding of NSMSs into power grids is the development trend. Due to the great difference of the steady-state and dynamic characteristics between NSMSs and synchronous generators (SG), it is necessary to study the voltage stability of power systems with a large number of NSMSs connected. In the traditional cognition of scholars, VSCs can provide voltage support for AC systems and be connected to passive networks [2]. Based on this cognition, the proportion of VSC-type power sources in a power system should be able to reach a high value or even 100%. However, in many power grids, it is found that the power grid cannot meet the requirement of the voltage stability when the proportion of VSC-type power sources is high to a certain extent. This phenomenon is at odds with the traditional cognition. In this paper, we analyze the voltage stability of power systems with NSMSs connected, and the research results can provide a theoretical basis for the stable operation of power systems with NSMSs connected.

For many power systems, the voltage instability has become the biggest threat to the safe operation. It is generally believed that the load with fast recovery characteristics is the main cause of the voltage instability [8]. The impact of load characteristics on the voltage stability has been the focus of academia and engineering in the past decades

* Corresponding author.
E-mail address: xuzheng007@zju.edu.cn (Z. Xu).

https://doi.org/10.1016/j.ijepes.2021.107087
Received 16 December 2020; Received in revised form 18 February 2021; Accepted 2 April 2021
Available online 20 April 2021
0142-0615/© 2021 Elsevier Ltd. All rights reserved.

[9,10]. With the increase of HVDC capacity and renewable energy, the impact of LCCs and VSCs on the voltage stability has gradually attracted the attention of scholars [11,12]. The influence of LCCs on the voltage stability is usually evaluated by the short-circuit ratio (SCR). The SCR is used by the CIGRE Working Group [13], and some new SCR calculation methods are proposed in recent years [14,15]. As for a power system fed by VSCs, a single-infeed VSC HVDC system model is established in [16], based on which the influence of NSMSs on the voltage stability is analyzed. Ref. [16] draws the conclusion that VSCs can provide better voltage-support to a weak receiving AC system than LCCs. In [17], the influence of VSCs on the voltage stability of a multi-infeed system is analyzed, it is shown that the AC voltage regulation in VSCs may adversely affect the dynamic performance of a weak AC system. The singular value theory can be applied to the voltage stability analysis of a power system fed by VSCs [18]. The singular value capability space proposed by [18] can indicate how much a VSC migrates the system away from the voltage instability. In [19], the interaction between LCCs and VSCs is analyzed based on a hybrid multi-infeed HVDC system model. According to the result in [19], LCCs will weaken the system strength for VSCs, and VSCs also weaken the system strength for LCCs. In most researches, the AC system is equivalent to a SG with impedance, while a detailed converter model is adopted [20]. Under this assumption, the voltage stability of a power system is equivalent to the voltage stability of the point of common coupling (PCC), the emphasis is on the interaction between the NSMS and the SG, while the interaction between the NSMS and the load is ignored. Voltage stability assessment methods for power systems with NSMSs connected are proposed in [21,22]. In [21], a global sensitivity analysis method is proposed to consider power system variabilities in the voltage stability evaluation. Compared with local sensitivity analysis, the global sensitivity analysis method is more accurate and the computation efficiency is improved. In [22], the impacts of the voltage-maintaining capacity and low-voltage tripping of distributed generation units on the static voltage stability of power systems are analyzed, and a distributed method is proposed to assess the voltage stability. In [23], the possibility of improving the voltage stability of power systems with large-scale NSMSs connected is discussed, and both active and reactive power injection of NSMSs are used to improve the voltage stability. Although many scholars have conducted in-depth research on the characteristics and control strategies of power systems with NSMSs connected, the interaction mechanism between various loads and NSMSs is still unclear, and further study is necessary.

A prominent advantage of the VSC is that it can be used for supplying power to passive systems [24], such as supplying power to passive islands. The basic passive control strategy of VSCs can refer to [2], and some improved passive control strategies have been proposed in recent years [25,26]. A control method that can improve the voltage quality of passive systems is put forward in [27]. The voltage quality of passive systems can also be improved by changing the reactive power control strategy [28,29]. Although the characteristic of VSCs can be as close to SGs as possible by applying reasonable control strategies, the VSC cannot be completely equivalent to a SG in the voltage stability analysis. Whether a passive system can maintain stable under disturbances, and whether the passive system with various loads can maintain stable, these issues remain to be studied.

The main contributions of this paper are summarized as follows:

(1) Based on the singularity of the Jacobian matrix, the impact of NSMSs on the small-disturbance voltage stability (SDVS) is analyzed. It is proved that there is a maximum allowable output for the NSMS. When the output of the NSMS exceeds the maximum allowable output, the power system will suffer from the small-disturbance voltage instability (SDVI).
(2) By judging whether there is a reasonable voltage solution for the power system in the transient process, the large-disturbance voltage instability (LDVI) mechanism of the power system with NSMSs connected is revealed.
(3) In passive systems, requirements of the voltage stability on load types and VSC parameters are put forward.

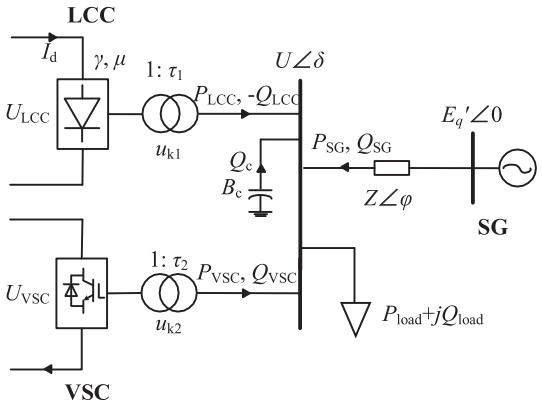

Fig. 1. The model of the power system with NSMSs connected.

The rest of this paper is organized as follows: Section 2 presents the modelling of the power system with NSMSs connected. In Section 3, the voltage stability of active systems with NSMSs connected is analyzed. The voltage stability of passive systems is studied in Section 4. Simulations are carried out in Section 5 and conclusions are provided in Section 6.

2. Modeling of active systems with NSMSs connected

To analyze the voltage stability of active systems with NSMSs connected, a simple power system model shown in Fig. 1 is adopted in this paper. In Fig. 1, the load is supplied by an LCC, a VSC and a SG. The mathematical model of the simple power system can be established as (1)–(15).

The Thevenin equivalent model is adopted to simulate the SG, that is, an equivalent impedance is connected in series with a voltage source. The output power of the SG are (1)–(2).

$$P_{SG} = \frac{1}{Z}\left[-U^2\cos\varphi + E_q^{'}U\cos(\delta+\varphi)\right] \tag{1}$$

$$Q_{SG} = \frac{1}{Z}\left[-U^2\sin\varphi + E_q^{'}U\sin(\delta+\varphi)\right] \tag{2}$$

Here, P_{SG} and Q_{SG} denote the output active power and reactive power of the SG, respectively; Z and φ represent the magnitude and phase angle of the equivalent impedance, respectively; U is the voltage magnitude of the AC bus; δ is the voltage phase angle of the AC bus; $E_q^{'}$ is the transient electromotive force of the SG.

The model of the LCC can be described as (3)–(8) [30]. The controller model of the LCC can be found in [30]. Expressions of the LCC active power and the LCC reactive power are described as (3) and (4), respectively. The positive direction of the power is shown in Fig. 1. In (3) and (4), C and K are two constants related to the parameters of the converter transformer. Eq. (5) is the expression of the direct current of the LCC. The output reactive power of the compensation capacitor is (8).

$$P_{LCC} = CU^2[\cos2\gamma - \cos(2\gamma+2\mu)] \tag{3}$$

$$Q_{LCC} = CU^2[2\mu + \sin2\gamma - \sin(2\gamma+2\mu)] \tag{4}$$

$$I_{dc} = KU[\cos\gamma - \cos(\gamma+\mu)] \tag{5}$$

$$C = \frac{3}{4\pi}\times\frac{S_T}{P_{dN}}\times\frac{1}{u_{k1}\%}\times\frac{1}{\tau^2} \tag{6}$$

$$K = \frac{1}{u_{k1}\%} \times \frac{1}{\tau} \tag{7}$$

$$Q_c = B_c U^2 \tag{8}$$

Here, P_{LCC} is the output active power by the LCC; Q_{LCC} is the reactive power absorbed by the LCC; P_{dN} is the rated active power of the LCC; I_{dc} is the direct current of the LCC; γ is the extinction angle of the LCC; μ is the commutation angle of the LCC; S_T is the capacity of the converter transformer; u_{k1} is the short-circuit ratio of the converter transformer; τ is the transformation ratio of the converter transformer; Q_c is the output reactive power of the compensation capacitor; B_c is the admittance of the compensation capacitor.

As for the VSC, assuming that the inner loop controller with a time scale of 10 ms can completely follow the current command values [31], then the model of the VSC can be established as (9)–(13) [32]. Eqs. (9) and (10) are expressions of the active power and the reactive power of the VSC. Eq. (11) describes the transformation relationship between the *dq* coordinate system and the *xy* coordinate system. Please refer to [32] for the controller model of the VSC.

$$P_{VSC} = UI_{VSC}\cos(\theta + \delta) \tag{9}$$

$$Q_{VSC} = UI_{VSC}\sin(\theta + \delta) \tag{10}$$

$$\begin{bmatrix} i_x \\ i_y \end{bmatrix} = \begin{bmatrix} \cos\theta_{PLL} & -\sin\theta_{PLL} \\ \sin\theta_{PLL} & \cos\theta_{PLL} \end{bmatrix} \begin{bmatrix} i_d \\ i_q \end{bmatrix} \tag{11}$$

$$\theta = \arctan(i_x / i_y) \tag{12}$$

$$I_{VSC} = \sqrt{i_x^2 + i_y^2} \tag{13}$$

Here, P_{VSC} and Q_{VSC} are active power and reactive power of the VSC; I_{VSC} is the magnitude of the AC current output by the VSC; θ is the phase angle of the AC current output by the VSC; i_x and i_y are the components of the AC current on *x*-axis and *y*-axis; i_d and i_q are the components of the AC current on *d*-axis and *q*-axis; θ_{PLL} is the output of the PLL.

The power balance equations of the AC bus are (14)–(15).

$$\Delta P = P_{VSC} + P_{LCC} + P_{SG} - P_{load} = 0 \tag{14}$$

$$\Delta Q = Q_{VSC} + Q_c + Q_{SG} - Q_{LCC} - Q_{load} = 0 \tag{15}$$

Here, P_{load} is the active power absorbed by the load; Q_{load} is the reactive power absorbed by the load; ΔP is the active power error; ΔQ is the reactive power error. The power flow solution problem of the power system can be summarized as follows: Seek the magnitude U and phase angle δ of the bus voltage so that the power errors (ΔP, ΔQ) are close enough or equal to zero.

3. Voltage stability analysis of active systems

3.1. SDVS analysis

The Jacobian matrix singularity can reflect the voltage stability of power systems, and the determinant value of the Jacobian matrix can be used as a voltage stability index, which is first pointed out by Venikov et al [33]. For the system model shown in Fig. 1, the linearized power flow equation is (16), then (17) can be used as a criterion for the voltage stability.

$$\begin{bmatrix} \Delta P \\ \Delta Q \end{bmatrix} = \boldsymbol{J} \begin{bmatrix} \Delta\delta \\ \Delta U \end{bmatrix} \tag{16}$$

$$\begin{cases} \det(J) > 0 & \text{stable} \\ \det(J) \le 0 & \text{unstable} \end{cases} \tag{17}$$

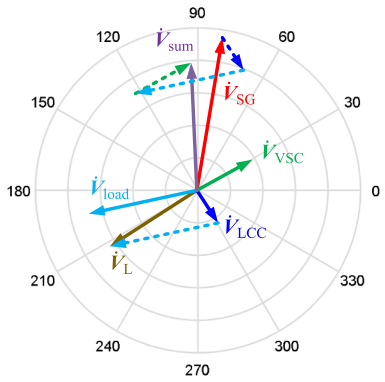

Fig. 2. Distribution of vectors related to the determinant values.

Here, $\Delta\delta$ is the correction amount of the bus voltage phase; ΔU is the correction amount of the bus voltage magnitude; $\boldsymbol{J}$ is the Jacobian matrix.

The time scales of the LCC constant direct current controller, the LCC constant extinction angel controller, the SG voltage controller, the VSC outer loop controller, and the VSC phase locked loop (PLL) are relatively long, all in the order of 100 ms or longer [30,31]. However, the response time of the AC bus voltage is very short, usually a few milliseconds. Therefore, controllers with long time scale are approximately neglected. On the premise that the above controllers have no time to respond, the expression of the Jacobian matrix can be written as (18), and the Jacobian matrix (18) is applicable to the SDVS analysis within 100 ms.

$$J = \begin{bmatrix} J_{p\delta} & J_{pv} \\ J_{q\delta} & J_{qv} \end{bmatrix} \tag{18}$$

Here,

$$J_{p\delta} = \frac{\partial \Delta P}{\partial \delta} = \frac{\partial P_{VSC}}{\partial \delta} + \frac{\partial P_{LCC}}{\partial \delta} + \frac{\partial P_{SG}}{\partial \delta} - \frac{\partial P_{load}}{\partial \delta}$$

$$J_{pv} = \frac{\partial \Delta P}{\partial U} = \frac{\partial P_{VSC}}{\partial U} + \frac{\partial P_{LCC}}{\partial U} + \frac{\partial P_{SG}}{\partial U} - \frac{\partial P_{load}}{\partial U}$$

$$J_{q\delta} = \frac{\partial \Delta Q}{\partial \delta} = \frac{\partial Q_{VSC}}{\partial \delta} + \frac{\partial Q_c}{\partial \delta} + \frac{\partial Q_{SG}}{\partial \delta} - \frac{\partial Q_{LCC}}{\partial \delta} - \frac{\partial Q_{load}}{\partial \delta}$$

$$J_{qv} = \frac{\partial \Delta Q}{\partial U} = \frac{\partial Q_{VSC}}{\partial U} + \frac{\partial Q_c}{\partial U} + \frac{\partial Q_{SG}}{\partial U} - \frac{\partial Q_{LCC}}{\partial U} - \frac{\partial Q_{load}}{\partial U}$$

By substituting (1)–(15) into (18), the determinant value of the Jacobian matrix is obtained as (19). See Appendices for the derivation process. In (19), S_{load} is the apparent power of the load; cosΦ is the power factor of the load.

$$\det(J) = U\left(\left|\dot{V}_{sum}\right|^2 - \left|\dot{V}_L\right|^2\right) \tag{19}$$

Here,

$$\dot{V}_{sum} = \dot{V}_{VSC} + \dot{V}_{SG} + \dot{V}_{LCC} + \dot{V}_{load}$$

$$\dot{V}_L = \dot{V}_{LCC} + \dot{V}_{load}$$

$$\dot{V}_{VSC} = I_{VSC}\angle(\theta + \delta)$$

$$\dot{V}_{SG} = \frac{E_q^{'}}{Z}\angle(\delta + \varphi)$$

$$\dot{V}_{LCC} = \frac{2\sqrt{2}CI_d}{K}\angle(-\gamma - \mu)$$

$$\dot{V}_{load} = \frac{S_{load}}{U}\angle(\pi + \Phi)$$

Because the voltage magnitude is always larger than zero, it can be seen from (19) that the sign of the determinant value depends on the magnitude relationship between $\dot{V}_{sum}$ and $\dot{V}_L$. The magnitude of $\dot{V}_{sum}$ depends on the parameters of the VSC, the SG, the LCC and the load. The magnitude of $\dot{V}_L$ is determined by the parameters of the LCC and the load. The distribution of $\dot{V}_{sum}$ and $\dot{V}_L$ is plotted in Fig. 2. The influence of each component on the determinant value is also shown in Fig. 2. For example, the greater the magnitude of $\dot{V}_{SG}$ is, the greater the magnitude of $\dot{V}_{sum}$ is, which means that increasing the AC system strength can increase the determinant value of the Jacobian matrix. Similarly, $\dot{V}_{VSC}$ is located in the first quadrant, which is the same as $\dot{V}_{SG}$. This shows that increasing the output power of the VSC can also increase the determinant value of the Jacobian matrix. On the contrary, increasing the magnitude of $\dot{V}_{load}$ will increase the magnitude of $\dot{V}_L$ and decrease the magnitude of $\dot{V}_{sum}$, which means that the determinant value of the Jacobian matrix will decrease with the load increasing.

In addition, $\dot{V}_{LCC}$ is located in the fourth quadrant, affecting $\dot{V}_{sum}$ and $\dot{V}_L$ at the same time. Therefore, the effect of the LCC on the determinant value of the Jocabian matrix is difficult to determine. The effect of the LCC on the SDVS is related to the operating parameters. The LCC is both an active power source and a reactive load. As the former, the LCC is beneficial to improve the SDVS, but as the latter, the LCC will deteriorate the SDVS. Although the reactive power absorbed by the LCC is completely compensated by the compensation capacitor, the reactive power absorbed by the LCC will still deteriorate the SDVS due to the rapid power recovery characteristics.

It should be noted that the above analysis are based on the premise that the system strength and the load remain unchanged. However, in reality, the connection of the NSMS is usually to compensate for increasing load or replace original SGs, which means that the increase of the NSMS is accompanied by load increasing or system strength weakening. In the following, the impact of the NSMS on the SDVS will be studied under the scenario where the load is variable.

3.2. Maximum allowable output of NSMSs

In the simple power system shown in Fig. 1, the active power balance equation is (20). The output apparent power of the VSC is S_{VSC}, the power factor of the VSC is $\cos(\theta + \delta)$, therefore (20) can be rewritten as (21).

$$P_{load} = P_{SG} + P_{LCC} + P_{VSC} \tag{20}$$

$$S_{load} = \frac{P_{SG} + P_{LCC}}{\cos\Phi} + \frac{S_{VSC}\cos(\theta + \delta)}{\cos\Phi} \tag{21}$$

The relationship between the apparent power and the output current is (22).

$$I_{VSC} = \frac{S_{VSC}}{U} \tag{22}$$

According to (17), the determinant value of the Jacobian matrix is zero when the system is critical stable. Substituting (21) and (22) into (19), the determinant value of the Jacobian matrix is (23) when the system is critical stable.

$$\det(J) = a_0 S_{VSC}^2 + a_1 S_{VSC} + a_2 = 0 \tag{23}$$

Here,

$$a_0 = \frac{1}{U} - \frac{2\cos(\theta + \delta)\cos(\theta + \delta - \Phi)}{U\cos\Phi}$$

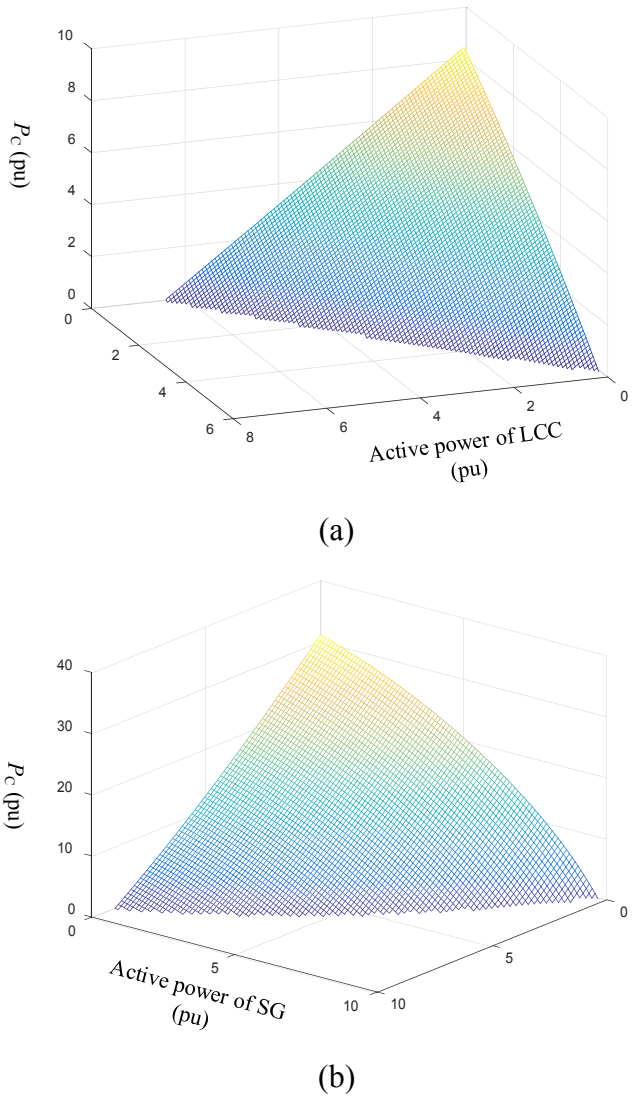

Fig. 3. P_C versus P_{SG} and P_{LCC}. (a) The condition when the constant power load model is adopted. (b) The condition when the constant current load model is adopted.

$$a_1 = \frac{2E_q^{'}}{Z}\cos(\theta - \varphi) + \frac{4CI_d}{K}\cos(\gamma + \mu + \theta + \delta) - \frac{2(P_{SG} + P_{LCC})}{U\cos\Phi}\cos(\theta + \delta - \Phi) - \frac{2E_q^{'}\cos(\theta + \delta)\cos(\delta + \varphi - \Phi)}{Z\cos\Phi}$$

$$a_2 = \frac{E_q^{'2}U}{Z^2} + \frac{4CUI_dE_q^{'}}{KZ}\cos(\gamma + \mu + \delta + \varphi) - \frac{2(P_{SG} + P_{LCC})E_q^{'}}{Z\cos\Phi}\cos(\delta + \varphi - \Phi)$$

It is assumed that the bus voltage can be kept at the rated value under various steady-state conditions. On the premise that the bus voltage is equal to the rated value, (23) is a quadratic equation of one variable for S_{VSC}. Solving (23) and taking the positive root, the expression of the S_{VSC} when the system is critical stable can be obtained as (24). The critical active power P_C of the VSC is (25). When the output active power of the VSC exceeds P_C, the determinant value of the Jacobian matrix will be less than zero, indicating that the system is in SDVI.

$$S_C = \frac{-a_1 - \sqrt{a_1^2 - 4a_0a_2}}{2a_0} \tag{24}$$

$$P_C = S_C\cos(\theta + \delta) \tag{25}$$

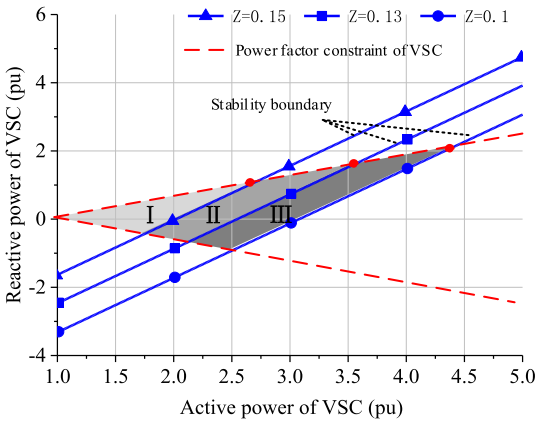

Fig. 4. Safe region of the VSC.

By changing the active power of the SG and the LCC, the change of P_C can be obtained as shown in Fig. 3a. In Fig. 3a, the results are shown by unit values, and the base capacity is 100 MVA. The system parameters are shown in Table B1 in Appendices. It can be seen from Fig. 3a that the load cannot be increased without limit even if the load is compensated locally by the NSMS. Under the SDVS constraint, both the LCC and the VSC have a maximum allowable output.

In the above analysis, the constant power load model is adopted. If the constant current model is adopted, we can get P_C as shown in Fig. 3b. Similarly, the base capacity of the Fig. 3b is also 100 MVA. By comparing Fig. 3a and Fig. 3b, it can be seen that P_C is significantly increased when the constant current model is adopted. In addition, there is no real number solution for (23) if the load keeps constant impedance, which indicates that the maximum allowable output does not exist. In this case, the system can always keep SDVS no matter how large the NSMS output is. Among the three load models of constant power, constant current, and constant impedance, the constant impedance load has the strongest voltage regulation capability, which can significantly improve the SDVS. The voltage regulation capability of the constant power load is the weakest, and the P_c is the smallest when the constant power load is adopted.

The results in Fig. 3 are obtained when the power factor of the VSC is 1.0. Considering that the VSC can generate reactive power, the safe operating region of the VSC will be studied below. When the system is critical stable, the VSC reactive power versus the VSC active power can be obtained by solving (23), as shown in Fig. 4. In Fig. 4, the results are shown by unit values, and the base capacity is 100 MVA. If the operating point of the VSC is located in the region above the stability boundary, the system can keep SDVS. On the contrary, the system will be unstable when the operating point of the VSC is below the stability boundary. Theoretically, as long as the VSC outputs enough reactive power, the active power of the VSC can be increased unlimited, and P_C will not exist. However, considering the limitation of the power factor, the safe operating regions of the VSC are region I-III shown in Fig. 4. When the equivalent impedance Z of the AC system is 0.15, the safe operating region is region I. When Z is 0.13, the safe operating regions are region I and region II. When Z is 0.1, the safe operating regions are region I, region II and region III.

Through the above SDVS analysis, the following conclusions can be drawn:

(1) The SDVS of a power system with the NSMS connected is related to the static characteristic of load.
(2) If the static characteristic of the load is close to constant impedance, the system can always keep SDVS.
(3) If the static characteristic of the load is close to constant power or constant current, the output of the NSMS cannot be increased without limit in order to guarantee the SDVS of the power system.

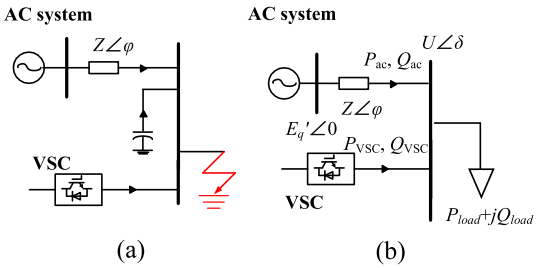

Fig. 5. The system equivalent circuit during the transient process. (a) The system equivalent circuit during fault. (b) The system equivalent circuit at the moment of fault clearing.

3.3. LDVS analysis

In this subsection, the impact of the NSMS on the LDVS will be studied. For the simple system shown in Fig. 1, we assume that a three-phase grounding fault occurs at the AC bus. The transient process can be divided into two stages. The first stage is during the fault, and the second stage is the recovery stage after the fault is cleared. The dynamic characteristics of the system in the two stages are introduced below.

Firstly, the first stage is introduced. Considering the communication delay and the circuit breaker action time, there is usually a certain delay from the fault occurrence to the fault clearing. The time from the fault occurrence to the fault clearing is the first stage. When a three-phase grounding short-circuit fault exists in the system, the commutation failure will occur in the LCC, the active power and the reactive power of the LCC are reduced to zero. Therefore, in the first stage, the LCC is equivalent to being disconnected. The system equivalent circuit is shown as Fig. 5(a). In the first stage, the excitation system of the SG will act in an attempt to increase the bus voltage. The differential equation of the transient electromotive force is (26). To simplify the derivation, the d-axis reactance is assumed to be equal to the q-axis reactance, that is $x_q = x_d = x_d^{'}$. Since the bus voltage is at a very low level in the first stage, the excitation system is usually in the top excitation state, as (27) shows. By solving (26), the expression of the transient electromotive force in the first stage can be obtained as (28).

$$\frac{dE_q^{'}}{dt} = \frac{1}{T_d^{'}}\left[E_{fd} - E_q^{'} - \left(x_d - x_d^{'}\right)i_{dg}\right] \tag{26}$$

$$E_{fd} = V_{Rmax} \tag{27}$$

$$E_q^{'}(t) = V_{Rmax} + \left[E_q^{'}(0) - V_{Rmax}\right]e^{-\frac{t}{T_d^{'}}} \tag{28}$$

Here, $T_d^{'}$ is the transient time constant of the SG; E_{fd} is the excitation electromotive force of the SG; x_d is the d-axis synchronous reactance of the SG; $x_d^{'}$ is the d-axis transient reactance of the SG; i_{dg} is the d-axis current of the SG; V_{Rmax} is the maximum output limit of the excitation system.

In the first stage, the outer loop controller of the VSC is fully activated in an attempt to keep the output power unchanged, and the output current of the VSC will reach the maximum limit:

$$\sqrt{i_x^2 + i_y^2} = I_{VSC,\ Limit} \tag{29}$$

Here, $I_{VSC,\ Limit}$ is the maximum output limit of the AC current of the VSC.

Next, the dynamic characteristic of the system in the second stage is introduced. The second stage refers to the recovery stage that the system has not reached a steady-state point after the fault is cleared. In the second stage, the active power and reactive power of the LCC will gradually recover. Generally, the recovery speed of the reactive power is much faster than that of the active power. Therefore, it is conservative to

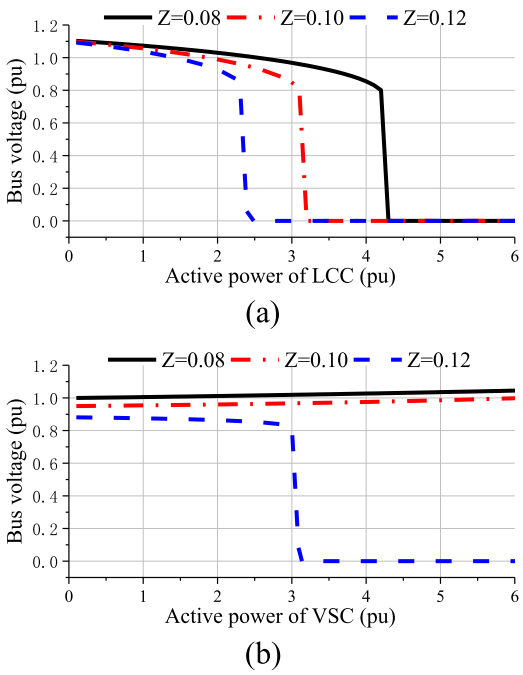

Fig. 6. The bus voltage at the moment of fault clearing. (a) The bus voltage versus the active power of the LCC. (b) The bus voltage versus the active power of the VSC.

assume that the reactive power absorbed by the LCC can be restored instantaneously after the fault is cleared, while the active power of the LCC will recover gradually from zero. Under this assumption, the voltage collapse is most likely to occur at the moment of fault clearing. At this moment, the reactive power absorbed by the LCC has recovered, and the active power output by the LCC is still zero. Therefore, the load of the SG is the largest at this moment, and the LDVI is most likely to occur. The system equivalent circuit at the moment of fault clearing is shown in Fig. 5 (b). If the first stage lasts for δt, the power flow equations at the moment of fault clearing are (30)–(31). The magnitude and phase of the bus voltage can be obtained by solving (30)–(31). If there is no positive real number solution for the voltage magnitude, the system is in LDVI.

$$\frac{1}{Z}\left[-U^2\sin\varphi+E_q^{'}(\Delta t)U\sin(\delta+\varphi)\right]+UI_{VSC,\,Limit}\sin(\delta+\theta)-Q_{load}=0 \tag{30}$$

$$\frac{1}{Z}\left[-U^2\cos\varphi+E_q^{'}(\Delta t)U\cos(\delta+\varphi)\right]+UI_{VSC,\,Limit}\cos(\delta+\theta)-P_{load}=0 \tag{31}$$

According to the above analysis of the two stages, the LDVS of the system can be judged by (30) and (31). In order to study the impact of the NSMS on the LDVS, we change the steady-state output of the NSMS and solve (30)–(31), the bus voltage at the moment of fault clearing versus the NSMS output can be obtained as shown in Fig. 6. In Fig. 6, the results are shown by unit values, and the base voltage is 525 kV. The system parameters can be found in Table B1 in Appendices. In Fig. 6, the abscissa shows the output active power of the NSMS at the initial steady-state point. When the output active power of the NSMS changes, the output of the SG will change accordingly to ensure that the power balance. The ordinate shows the bus voltage at the moment of fault clearing.

In Fig. 6(a), with the increase of the LCC output, the bus voltage decreases continuously, which indicates that the LDVS deteriorates.

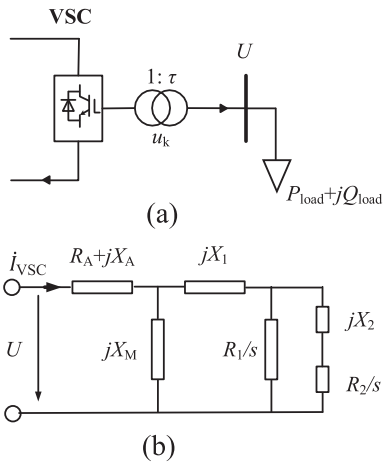

Fig. 7. The models of the passive system and the induction motor. (a) The passive system model. (b) The induction motor model.

When the output of the LCC is large enough, the bus voltage will collapse, which indicates that the system is in LDVI. Different from the LCC, the impact of the VSC on the LDVS is not fixed. In Fig. 6(b), when the equivalent impedance of the AC system Z is 0.08 or 0.1, the increase of the VSC output will increase the bus voltage, which is beneficial to the LDVS. However, when Z is 0.12, the increase of the VSC output will deteriorate the LDVS, even lead to the LDVI.

Under a severe short-circuit fault, the LCC commutation failure will occur, the load that should be supplied by the LCC will be transferred to the AC system, which increases the burden of the AC system and deteriorates the LDVS. The greater the LCC output, the greater the risk of the LDVI. The influence of the VSC on the LDVS is related to the system parameters. In a strong system, the increase of the VSC output will be beneficial to the LDVS, while the increase of the VSC output will deteriorate the LDVS in a weak system. The reason for this phenomenon is that the VSC presents the current source characteristic during the transient process. In a weak AC system, the bus voltage will be at a low level after clearing the fault, leading to the decrease of the VSC output. The load that should be supplied by the VSC will be transferred to the AC system, which will deteriorate the LDVS. If the AC system is strong, the bus voltage can be kept in a normal range after clearing the fault, the output of the VSC can be kept unchanged or even increased, which can reduce the burden of the AC system and improve the LDVS.

4. Voltage stability analysis of passive systems

In the above analysis, both the VSC and the LCC are fed into active systems. In this section, the voltage stability of passive systems will be analyzed. In the following, the passive system model shown in Fig. 7(a) will be adopted.

4.1. SDVS analysis

For a VSC, the difference between the passive control and the active control is that the control objectives of the outer loop controller and the PLL are different. Therefore, under the premise that the outer loop controller and the PLL are too slow to act, the model of the VSC can still be described by (9)–(13). With different static load models, the Jacobian matrix determinant values of the passive system are (32). The derivation process is similar to that in Section 3.1, which will not be repeated here. In (32), U is the magnitude of the bus voltage; P_{VSC} is the output active power of the VSC; Q_{VSC} is the output reactive power of the VSC.

$$\det(J)=\begin{cases}-\dfrac{P_{VSC}^2+Q_{VSC}^2}{U} & \text{constant power load}\\ 0 & \text{constant current load}\\ \dfrac{P_{VSC}^2+Q_{VSC}^2}{U} & \text{constant impedance load}\end{cases} \tag{32}$$

In (32), the bus voltage U is always larger than zero. Therefore, if the load keeps constant power, the determinant value of the Jacobian matrix will always be less than zero, and the passive system will be in SDVI according to the stability criterion in (17). As (32) shows, the determinant value of the Jacobian matrix will always be larger than zero if the load keeps constant impedance, which indicates that the system is always in SDVS. In addition, if the load keeps constant current, the Jacobian matrix determinant will be zero, indicating that the system is in critical SDVS.

4.2. LDVS analysis

During the transient process, due to the action of the outer loop controller and the PLL, the passively controlled VSC can be approximated as a voltage source before the output current reaches the limitation. If a fault is not severe enough to make the VSC output current reach the limitation, the characteristics of the VSC and the SG will be similar, and no more description will be given for this condition. However, under severe short-circuit faults, the output current of the VSC is usually limited by the maximum limiter, and the dynamic characteristics of the VSC will be quite different from that of the SG. In the following, the LDVS analysis of passive systems under severe short-circuit faults will be the focus. The induction motor load model is adopted to analyze the LDVS below. The equivalent circuit of the induction motor is shown in Fig. 7(b) In Fig. 7(b), X_M is the excitation reactance of the motor; R_A is the resistance of the motor stator; X_A is the reactance of the motor stator; R_1 is the resistance of the first rotor; X_1 is the reactance of the first rotor; R_2 is the resistance of the second rotor; X_2 is the reactance of the second rotor. If there is only one rotor in the motor, R_2 and X_2 are set as zero. The power absorbed by the induction motor is (33)–(34). In (33), I_{VSC} is the output current magnitude of the VSC; P_M is the active power absorbed by the induction motor; s is the slip of the induction motor; R_r is the equivalent resistance of the rotor. In (34), Q_M is the reactive power absorbed by the induction motor; X_r is the equivalent reactance of the rotor.

$$P_M(s)=I_{VSC}^2[R_r(s)+R_A] \tag{33}$$

$$Q_M(s)=I_{VSC}^2[X_r(s)+X_A] \tag{34}$$

Here,

$$R_r(s)+jX_r(s)=\left[\frac{R_1}{s}//\left(\frac{R_2}{s}+jX_2\right)+jX_1\right]//jX_M$$

The expression of the electromagnetic torque is (35). The load torque is assumed to be constant, then the rotor motion equation of the motor is (36).

$$T_e(s)=I_{VSC}^2R_r(s) \tag{35}$$

$$2H\frac{ds}{dt}=T_0-T_e(s) \tag{36}$$

Here, T_e is the electromagnetic torque of the motor; T_0 is the load torque of the motor; H is the rotor inertia time constant of the motor.

Assuming that a short-circuit fault occurs at the AC bus, the slip of the induction motor increases from s_0 to s_1 during the fault, and the VSC output current reaches the maximum limitation $I_{VSC,Limit}$. At the moment of fault clearing, the change rate of the slip is (37).

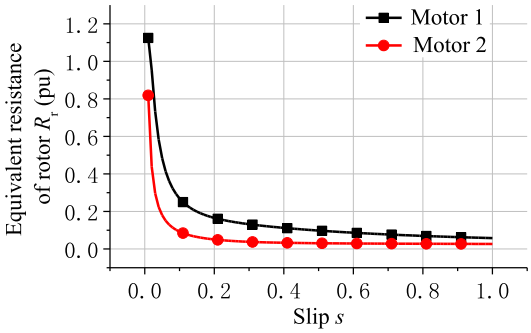

Fig. 8. The equivalent resistance versus the slip.

$$\frac{ds}{dt}=\frac{1}{2H}\left[T_0-I_{VSC,Limit}^2R_r(s_1)\right] \tag{37}$$

It should be noted that the equivalent resistance R_r decreases with the slip increasing, as Fig. 8 shows, the motor parameters and the bases can be found in Table B2 in Appendices. Therefore, if the VSC output current reaches the maximum limitation, the electromagnetic torque of the motor will decrease with the slip increasing. According to the relationship between the electromagnetic torque and the load torque, at the moment of fault clearing, three conditions can be summarized:

(1) $T_0 > T_e(s_1)$. At the moment of fault clearing, the change rate of the slip is larger than zero, the slip increases. The increasing slip will reduce the electromagnetic torque, leading to a further increase in the slip. The slip will increase until the motor is stalled.
(2) $T_0 < T_e(s_1)$. At the moment of fault clearing, the change rate of the slip is less than zero, the slip decreases. The decreasing slip will increase the electromagnetic torque, leading to a further decrease in the slip. The slip finally returns to a steady state point.
(3) $T_0 = T_e(s_1)$. This is a critical state, and the motor is critically stable.

In general, the stability of a power system is checked utilizing the most serious fault that may occur in the power system. If a three-phase metallic grounding short-circuit fault occurs at the bus, the electromagnetic torque of the motor will be zero during the fault, and the change rate of the slip is (38). Assuming that the fault occurs at moment t_0 and is cleared at moment t_1, and the initial value of the slip is s_0, then the slip at the moment t_1 will be (39).

$$\frac{ds}{dt}=\frac{T_0}{2H} \tag{38}$$

$$s_1=s_0+\frac{T_0}{2H}(t_1-t_0) \tag{39}$$

According to (39), when a three- phase metallic grounding fault occurs in the bus, the slip s_1 at the moment of fault clearing is only related to the load torque and the fault duration, and has nothing to do with the VSC. The load parameters are not determined by power system operators, it is not realistic to improve the LDVS by changing the motor parameters. For passive systems, a feasible way to improve the LDVS is to increase the VSC reserve capacity, that is to increase $I_{VSC,Limit}$. The larger $I_{VSC,Limit}$ is, the larger the electromagnetic torque is after the fault clearing, and the motor is less prone to be stalled.

5. Case study

In order to verify the above analysis results, simulations will be carried out in an active system and a passive system respectively. The simulation software is Power System Simulator/Engineering (PSS/E).

Table 1
Parameters of VSCs.

Items	VSC1	VSC2	VSC3
Rated capacity of single pole (MVA)	2000	1250	750
Number of poles	2	2	2
Rated DC voltage (kV)	500	500	500
Bridge arm reactance (mH)	32	32	66
Number of single bridge arm sub-modules	228	228	313
Sub-module capacitance (mF)	18	18	12

Table 2
Parameters of LCCs.

Items	Huaxin	Fengjing	Fengxian
Rated capacity of single pole (MVA)	1500	1500	3000
Number of poles	2	2	2
Rated DC voltage (kV)	500	500	800
Resistance of DC lines (Ω)	12.6	10.2	8.0

Table 3
Parameters of the VSCs in the passive system.

Items	VSC4	VSC5
Rated capacity (MVA)	400	800
Actual output active power (MW)	386	386
Rated DC voltage (kV)	500	500
Bridge arm reactance (mH)	66	66
Number of single bridge arm sub-modules	313	313
Sub-module capacitance (mF)	12	12

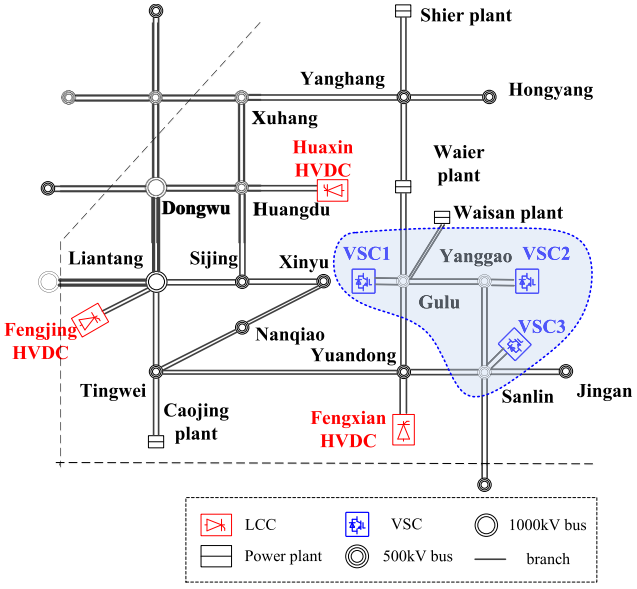

Fig. 9. The 500 kV network structure of the Shanghai power grid.

5.1. Active system

(1) *System description*: The planning data of the Shanghai power grid in the summer 2025 is adopted in this paper. The Shanghai power grid, originally comprising 15 buses of 500 kV, 66 branches of 500 kV, and three inverters of the LCC, is modified to include three inverters of the VSC. Parameters of the VSCs and LCCs are presented in Table 1, Table 2 and Table 3 respectively. The total load of the Shanghai power grid is about 34000 MW, and the installed capacity is about 20000 MW. In addition, the base voltage of the Shanghai power grid is 525 kV, and the base capacity of the Shanghai power grid is 100 MVA. The 500 kV network structure of the Shanghai power grid is shown in Fig. 9. The Shanghai power grid is a typical receiving end system, the power fed by LCCs accounts for 35% of the total load. All generators use 6th-order model (GENROU), with 4th-order excitation system (IEEET1). The comprehensive distribution network load model (CLODZN) and the two-terminal DC line model (CDC6T) are adopted in this paper. See PSS/E manual [34] for more details on the model of each device.

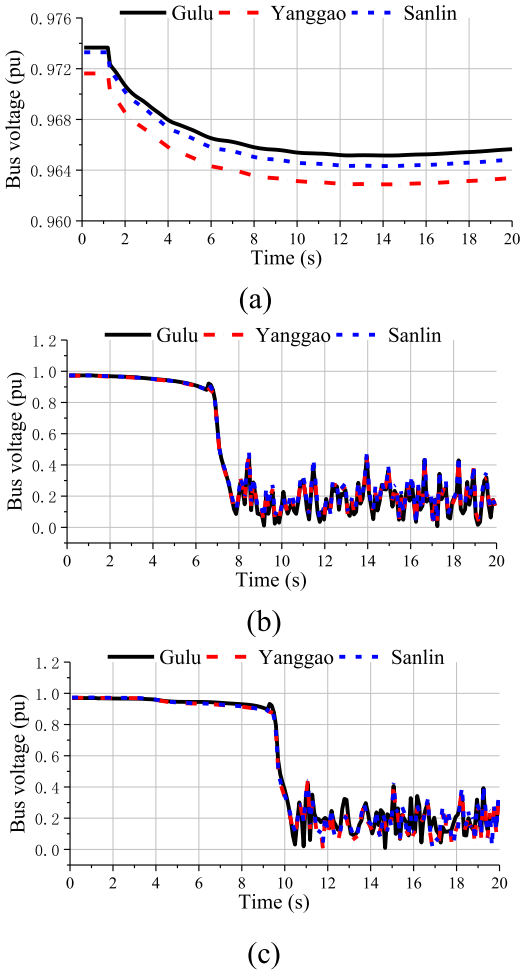

Fig. 10. Voltage curves under the small active load step. (a) Simulations results of the original system. (b) Simulation results under the condition that the VSCs adopt the d-axis constant active power controller and the q-axis constant reactive power controller. (c) Simulation results under the condition that the VSCs adopt the d-axis constant DC voltage controller and the q-axis constant AC voltage controller.

(2) *SDVS analysis*: The ZIP load model is adopted for the SDVS analysis, consisting of 60% constant power load and 40% constant impedance load. In the original system, if a 1% active load step occurs at bus Sanlin, the bus voltage curves can be obtained as shown in Fig. 10(a). According to Fig. 10(a), the Shanghai power grid is in SDVS. Considering the future load growth and the rapid development of the offshore wind power, we assume that the loads in Gulu, Yanggao and Sanlin will be increased in equal proportion, and the increased loads are fully compensated by VSCs locally, as shown in the shaded part in Fig. 9. Since the increased loads are compensated by VSCs locally, the load growth will not affect the power flow of the Shanghai power grid. The power flow of the modified system is completely consistent with that of the original system. When the loads increase to twice of

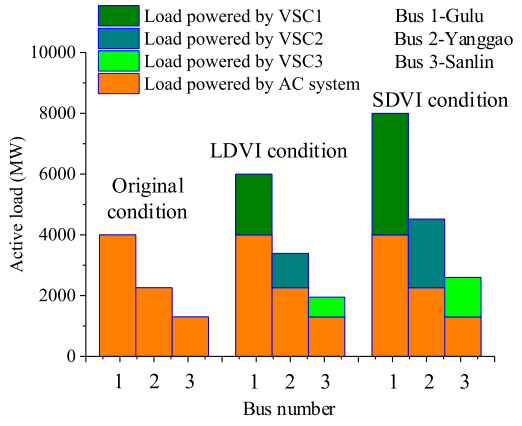

Fig. 11. Values of the load and the VSC output.

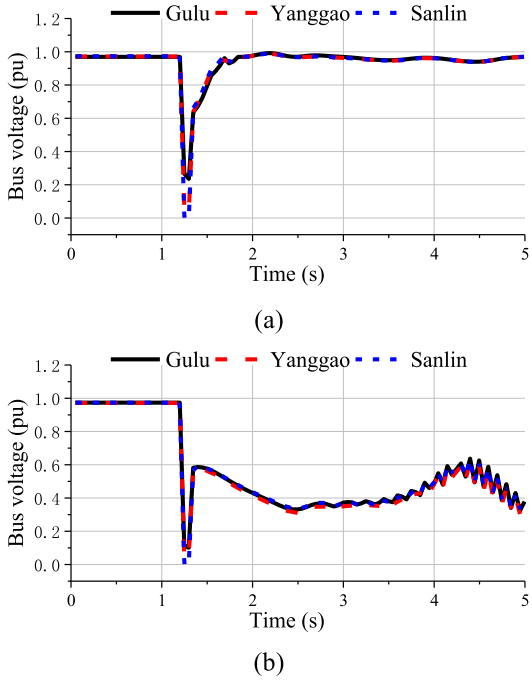

Fig. 12. Simulation results under the short-circuit fault. (a) Voltage curves of the original system. (b) Voltage curves of the modified system.

the original, the same active load disturbance is applied at bus Sanlin, and the bus voltage curves can be obtained as shown in Fig. 10(b). It can be seen from Fig. 10(b) that a small load step leads to the voltage collapse, which indicates that the system is in SDVI. In Fig. 10(b), the control mode of the *d*-axis constant active power and the *q*-axis constant reactive power is adopted for the three VSCs. In order to illustrate the influence of the control strategy on the SDVS, the control mode of the *d*-axis constant DC voltage and the *q*-axis constant AC voltage is adopted, and the simulation results are shown in Fig. 10(c). It can be seen from Fig. 10(c) that the system is also in SDVI. Under the SDVI

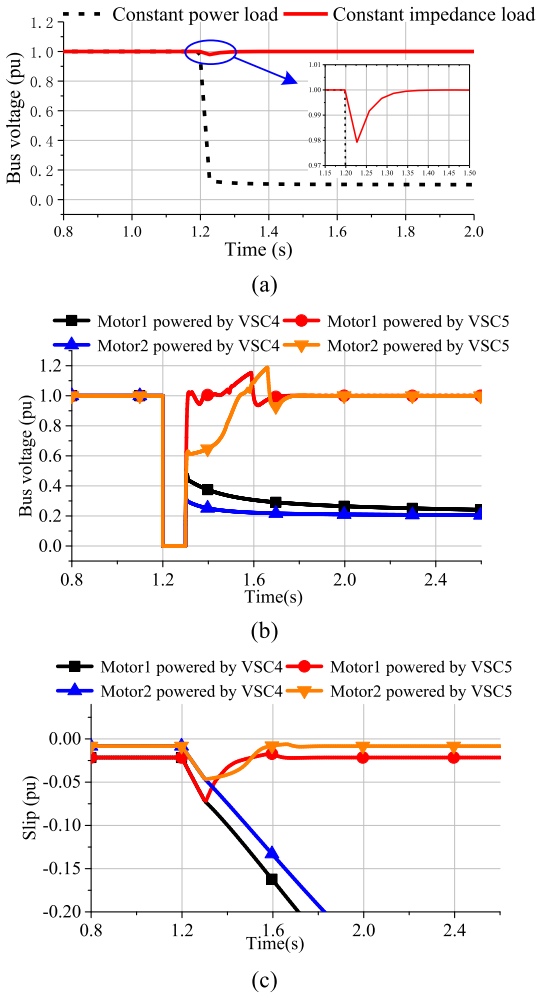

Fig. 13. Simulation results in a passive system. (a) Voltage curves under the small active load step. (b) Voltage curves under the short-circuit fault. (c) Slip curves under the short-circuit fault.

condition, the values of the loads and the VSC output can be found in Fig. 11.

Before and after the system is modified, the AC system strength and the power flow have not changed. However, it can be seen from Fig. 10 that the load increase deteriorates the SDVS. When the load in Gulu, Yanggao and Sanlin is twice that of the original, the system is in SDVI. This indicates that for the Shanghai power grid, there is a maximum allowable VSC output, and the SDVI will occur when the VSC output exceeds the maximum allowable value.

(3) *LDVS analysis*: The comprehensive load model is adopted for the LDVS analysis, consisting of 40% induction motor load, 20% constant power load and 40% constant impedance load. The fault is set as a three-phase grounding short-circuit fault at the Yuandong-Sanlin double branches. At 1.2 s, the fault occurs in the middle of one branch and lasts for 0.1 s. At 1.3 s, the fault is cleared. In the original system, the simulation results is shown in

Fig. 12(a). In Fig. 12(a), the voltage of each bus can quickly return to a normal value after the fault is cleared, which indicates that the system is in LDVS. Similarly, the loads in Gulu, Yanggao and Sanlin are increased in equal proportion, and the increased load is fully compensated by VSCs locally. When the load increases to 1.5 times of the original, the same fault is applied and the simulation results are shown in Fig. 12(b). As can be seen from Fig. 12(b), the voltage cannot recover to the normal range after the fault is cleared, which indicates that the system is in LDVI. Under the LDVI condition, the values of the loads and the VSC output can be found in Fig. 11.

Comparing Fig. 12(a) and Fig. 12(b), it can be seen that the LDVS of the system still deteriorates even if the VSC compensates the increased load. When the loads in Gulu, Yanggao and Sanlin are 1.5 times that of the original, the system is in LDVI. This phenomenon can be understood as that when the VSC supplies a load with fast recovery characteristics, the help of the SG is necessary to maintain voltage stability. However, the help provided by the SG is limited. With the increase of the load and the VSC capacity, the voltage stability margin of the system continues to decline.

5.2. Passive system

The structure of the passive system is shown in Fig. 7. The SDVS of the passive system is first analyzed, and the system parameters can be found in Table 3 (VSC4). The simulation is carried out under two load models, one is the constant power model and the other is the constant impedance model. A 1% active load step is selected as the disturbance, the simulation results are shown in Fig. 13(a). It can be seen from Fig. 13 (a) that in a passive system, it is impossible for the VSC to supply a constant power load stably, a small disturbance will cause the bus voltage collapse.

Then the LDVS of the passive system is analyzed, the induction motor model is adopted for the load. In order to explain the influence of the system parameters on the LDVS, four sets of system parameters are selected. Set 1: motor1 powered by VSC4, set 2: motor 2 powered by VSC4, set 3: motor 1 powered by VSC5, set 4: motor 2powered by VSC5. See Table 3 for VSC parameters, and Table B2 in Appendices for motor parameters. The fault is set as a three-phase grounding short-circuit fault at the PCC, the fault occurs at 1.2 s and is cleared after 0.1 s. The simulation results under the four sets of system parameters are shown in Fig. 13(b)–(c). When the rated capacity of the VSC is 400 MVA (VSC4), the short-circuit fault will cause the motor to be stalled and the system voltage will collapse. If the rated capacity of the VSC is increased to 800 MVA (VSC5), the motor can be restored to a steady-state operating point, and the system can be kept LDVS. In addition, the AC voltage recovery characteristics under motor1 are significantly better than those under motor2. It can be concluded that sufficient VSC reserve capacity is necessary for a passive system if the load is an induction motor. When the VSC reserve capacity is insufficient, the passive system will have the risk of the LDVI.

6. Conclusions

On the basis of a simple power system model, the impact of the NSMS on the voltage stability is analyzed, which can provide guidance for power grids planning. Conclusions are drawn as follows.

(1) In a power system dominated by the constant power load or the constant current load, the output of the LCC or the VSC cannot be increased unlimited. When the active power of the LCC or the VSC exceeds the maximum allowable output, the system will be in SDVI.
(2) Due to the commutation failure of the LCC, there is a maximum allowable output for the LCC under the LDVS constraint. When the active power of the LCC exceeds the maximum allowable output, the system will be in LDVI. The impact of the VSC on the LDVS is related to the system strength. In a strong system, the increase of the VSC output will benefit the LDVS, while the increase of the VSC output will deteriorate the LDVS in a weak system.
(3) In passive systems, if the load exhibits the characteristic of constant power, then the system is in SDVI. If the load exhibits the characteristic of constant current or constant impedance, the system will be stable under small disturbances.
(4) In passive systems, if the load is an induction motor, sufficient reserve capacity of the VSC is necessary to prevent the LDVI. When the reserve capacity of the VSC is insufficient, the induction motor is easy to be stalled under short-circuit faults.

CRediT authorship contribution statement

Guoteng Wang: Conceptualization, Methodology, Software, Visualization, Writing - original draft, Formal analysis. **Zheng Xu:** Supervision, Project administration, Resources, Data curation, Writing - review & editing. **Zheren Zhang:** Validation, Investigation.

Declaration of Competing Interest

The authors declare that they have no known competing financial interests or personal relationships that could have appeared to influence the work reported in this paper.

Appendix A

A. *Determinant value of the Jacobian matrix:* The derivation process of the Jacobian matrix determinant value is presented.

$$\det(J) = J_{p\delta}J_{qv} - J_{pv}J_{q\delta} \tag{A1}$$

Here,

$$J_{p\delta} = \frac{\partial \Delta P}{\partial \delta} = -UI_{VSC}\sin(\theta+\delta) - \frac{E_q^{'}U}{Z}\sin(\delta+\varphi)$$

$$J_{pv} = \frac{\partial \Delta P}{\partial U} = I_{VSC}\cos(\theta+\delta) + 2CUK_P(\gamma,\ \mu) +$$

$$CU^2\frac{\partial K_P(\gamma,\ \mu)}{\partial \mu}\frac{\partial \mu}{\partial U} - \frac{2U}{Z}\cos\varphi + \frac{E_q^{'}}{Z}\cos(\delta+\varphi)$$

$$J_{q\delta} = \frac{\partial \Delta Q}{\partial \delta} = UI_{VSC}\cos(\theta+\delta) + \frac{E_q^{'}U}{Z}\cos(\delta+\varphi)$$

$$J_{qv} = \frac{\partial \Delta Q}{\partial U} = I_{VSC}\sin(\theta+\delta) + 2B_cU - 2CUK_Q(\gamma,\ \mu) - CU^2\frac{\partial K_Q(\gamma,\ \mu)}{\partial \mu}\frac{\partial \mu}{\partial U} - \frac{2U}{Z}\sin\varphi + \frac{E_q^{'}}{Z}\sin(\delta+\varphi)$$

$$\frac{\partial K_Q(\gamma,\ \mu)}{\partial \mu} = 2 - 2\cos(2\gamma+2\mu) = 4\sin^2(\gamma+\mu)$$

$$\frac{\partial K_P(\gamma,\ \mu)}{\partial \mu} = 2\sin(2\gamma+2\mu) = 4\sin(\gamma+\mu)\cos(\gamma+\mu)$$

$$\frac{\partial \mu}{\partial U} = -\frac{1}{\sqrt{1-\left(\cos\gamma - \frac{I_d}{KU}\right)^2}} \times \frac{I_d}{KU^2} = -\frac{1}{\sin(\gamma+\mu)} \times \frac{I_d}{KU^2}$$

Eq. (A2) can be obtained by expanding (A1).

$$\det(J) = -UI_{VSC}^2 + \frac{E_q^{'2}U}{Z^2} + 2\left[\frac{U^2\sin\varphi - UE_q^{'}\sin(\delta+\varphi)}{Z} + CU^2K_Q(\gamma,\ \mu) - B_cU^2 + \frac{CU^3}{2}\frac{\partial K_Q(\gamma,\ \mu)}{\partial \mu}\frac{\partial \mu}{\partial U}\right] \times \left[I_{VSC}\sin(\theta+\delta) + \frac{E_q^{'}}{Z}\sin(\delta + \varphi)\right] + 2\left[\frac{U^2\cos\varphi - UE_q^{'}\cos(\delta+\varphi)}{Z} - CU^2K_P(\gamma,\ \mu) - \frac{CU^3}{2}\frac{\partial K_P(\gamma,\ \mu)}{\partial \mu}\frac{\partial \mu}{\partial U}\right]\left[I_{VSC}\cos(\theta+\delta) + \frac{E_q^{'}}{Z}\cos(\delta+\varphi)\right] \quad (A2)$$

The power flow Eqs. (14)–(15) can be rewritten as (A3)–(A4).

$$-\frac{U^2\sin\varphi - UE_q^{'}\sin(\delta+\varphi)}{Z} + B_cU^2 + UI_{VSC}\sin(\theta+\delta) - CU^2K_Q(\gamma,\ \mu) - Q_{load} = 0 \quad (A3)$$

$$-\frac{U^2\cos\varphi - UE_q^{'}\cos(\delta+\varphi)}{Z} + CU^2K_P(\gamma,\ \mu) + UI_{VSC}\cos(\theta+\delta) - P_{load} = 0 \quad (A4)$$

Eq. (A5) can be obtained by substituting (A3) and (A4) into (A2).

$$\det(J) = \frac{E_q^{'2}U}{Z^2} + UI_{VSC}^2 + \frac{2E_q^{'}UI_{VSC}}{Z}\cos(\theta-\varphi) + \frac{4CUI_dI_{VSC}}{K}\cos(\gamma+\mu+\theta+\delta) + \frac{4CUI_dE_q^{'}}{KZ}\cos(\gamma+\mu+\delta+\varphi) - 2S_{load}I_{VSC}\cos(\theta+\delta-\Phi) - \frac{2S_{load}E_q^{'}}{Z}\cos(\delta+\varphi-\Phi) \quad (A5)$$

By further simplifying (A5), we can obtain (A6).

$$\det(J) = U\left|I_{VSC}\angle(\theta+\delta) + \frac{E_q^{'}}{Z}\angle(\delta+\varphi) + \frac{2CI_d}{K}\angle(-\gamma-\mu) + \frac{S_{load}}{U}\angle(\pi+\Phi)\right|^2 - U\left|\frac{2CI_d}{K}\angle(-\gamma-\mu) + \frac{S_{load}}{U}\angle(\pi+\Phi)\right|^2 \quad (A6)$$

B. Parameters:

See Tables B1 and B2.

Table B1
Parameters of the simple power system.

Items	Value
Transient electromotive force $E_q^{'}$ (pu)	1.1
The equivalent impedance of AC system Z (pu)	0.1
Active power output by the SG P_{AC} (pu)	2.0
Active power output by the LCC P_{LCC} (pu)	2.0
Active power output by the VSC P_{VSC} (pu)	1.0
Power factor of the VSC	1.0
Power factor of the load	0.95
Parallel admittance B_c (pu)	1.11
Maximum output limit of the excitation system V_{Rmax} (pu)	4.0
Transient time constant $T_d^{'}$ (s)	7.8
Capacity base (MVA)	100
AC voltage base (kV)	525

Table B2
Typical parameters of two motors.

Items	Motor1	Motor2
Capacity (MVA)	400	400
Voltage base (kV)	35	35
Initial absorbed active power (MW)	386	386
R_A (pu)	0.0369	0.0138
L_A (pu)	0.1318	0.083
L_M (pu)	2.396	3.0
R_1 (pu)	0.0645	0.055
L_1 (pu)	0.0415	0.053
R_2 (pu)	0.0489	0.0115
L_2 (pu)	0.321	0.055
H (pu)	0.6	1.0
Load Damping Factor (pu)	1.0	1.0
Initial Slip	−0.02149	−0.00837

References

[1] Zhang L, Harnefors L, Nee H. Power-synchronization control of grid-connected voltage-source converters. IEEE Trans Power Syst 2010;25(2):809–20.
[2] Zhang L, Harnefors L, Nee H. Modeling and Control of VSC-HVDC Links Connected to Island Systems. IEEE Trans Power Syst May 2011;26(2):783–93.
[3] Rodriguez P, Pou J, Bergas J, Candela JI, Burgos RP, Boroyevich D. Decoupled double synchronous reference frame PLL for power converters control. IEEE Trans Power Electron March 2007;22(2):584–92.
[4] Liu Z, Yu J, Guo X, Sun T, Zhang J. Survey of technologies of line commutated converter based high voltage direct current transmission in China. CSEE J Power Energy Syst 2015;1(2):1–8.
[5] Xu L, Yao L, Sasse C. Grid integration of large DFIG-based wind farms using VSC transmission. IEEE Trans Power Syst 2007;22(3):976–84.
[6] Bresesti P, Kling WL, Hendriks RL, Vailati R. HVDC connection of offshore wind farms to the transmission system. IEEE Trans Energy Convers 2007;22(1):37–43.
[7] Lu S, Xu Z, Xiao L, Jiang W, Bie X. Evaluation and enhancement of control strategies for VSC stations under weak grid strengths. IEEE Trans Power Syst 2018; 33(2):1836–47.
[8] Hill DJ. Nonlinear dynamic load models with recovery for voltage stability studies. IEEE Trans Power Syst 1993;8(1):166–76.
[9] Huang W, Hill DJ. Network-based analysis of long-term voltage stability considering loads with recovery dynamics. Int J Electr Power Energy Syst 2020; 119.
[10] Rodriguez-Garcia L, Perez-Londono S, Mora-Florez J. An optimization-based approach for load modelling dependent voltage stability analysis. Int. J. Electr. Power Energy Syst. 2019;177.
[11] Xu J, et al. An on-line power/voltage stability index for multi-infeed HVDC systems. J Mod Power Syst Clean Energy 2019;7(5):1094–104.
[12] Renedo J, García-Cerrada A, Rouco L. Reactive-power coordination in VSC-HVDC multi-terminal systems for transient stability improvement. IEEE Trans Power Syst 2017;32(5):3758–67.
[13] CIGRE Working Group B4.41. Systems with multiple DC infeed [R]. Paris: CIGRE; 2008.
[14] Lee DHA, Andersson G. An equivalent single-infeed model of multi-infeed HVDC systems for voltage and power stability analysis. IEEE Trans Power Deliv 2016;31 (1):303–12.
[15] Zhang F, Xin H, Wu D, Wang Z, Gan D. Assessing strength of multi-infeed LCC-HVDC systems using generalized short-circuit ratio. IEEE Trans Power Syst 2019; 34(1):467–80.
[16] Aik DLH, Andersson G. Fundamental analysis of voltage and power stability of single-infeed voltage-source converter HVDC systems. IEEE Trans Power Deliv 2019;34(1):365–75.
[17] Shah R, Preece R, Barnes M. The impact of voltage regulation of multiinfeed VSC-HVDC on power system stability. IEEE Trans Energy Convers 2018;33(4):1614–27.
[18] Urquidez OA, Xie L. Singular value sensitivity based optimal control of embedded VSC-HVDC for steady-state voltage stability enhancement. IEEE Trans Power Syst 2016;31(1):216–25.
[19] Ni X, Gole AM, Zhao C, Guo C. An improved measure of AC system strength for performance analysis of multi-infeed HVdc systems including VSC and LCC converters. IEEE Trans Power Deliv 2018;33(1):169–78.
[20] Chen J, Milano F, O'Donnell T. Assessment of grid-feeding converter voltage stability. IEEE Trans Power Syst 2019;34(5):3980–2.
[21] Xu X, Yan Z, Shahidehpour M, Wang H, Chen S. Power system voltage stability evaluation considering renewable energy with correlated variabilities. IEEE Trans Power Syst 2018;33(3):3236–45.
[22] Li Z, Guo Q, Sun H, Wang J, Xu Y, Fan M. A distributed transmission-distribution-coupled static voltage stability assessment method considering distributed generation. IEEE Trans Power Syst 2018;33(3):2621–32.
[23] Kawabe K, Ota Y, Yokoyama A, Tanaka K. Novel dynamic voltage support capability of photovoltaic systems for improvement of short-term voltage stability in power systems. IEEE Trans Power Syst 2017;32(3):1796–804.
[24] Guibin Zhang, Zheng Xu, Hongtao Liu. Supply passive networks with VSC-HVDC. In: 2001 power engineering society summer meeting. Conference proceedings (Cat. No.01CH37262), Vancouver, BC, Canada, vol.1; 2001. p. 332–336.
[25] Chen D, Hu Y, Wang X, Shen F, Teng Y. Control strategy of VSC-HVDC inverter supplying power to the isolated grid with induction motor. In: 2017 China international electrical and energy conference (CIEEC), Beijing; 2017. p. 497–503.
[26] Wu X, Mei J, Wang B, Liang D, Qin C, Zong J. Unbalanced loads control strategy for virtual synchronous generator in passive network. In: 2019 IEEE innovative smart grid technologies – Asia (ISGT Asia), Chengdu, China; 2019. p. 2063–68.
[27] Tang X, Lu DD. Enhancement of voltage quality in a passive network supplied by a VSC-HVDC transmission under disturbances. Int J Electr Power Energy Syst 2014; 54:45–54.
[28] Xu H, Zhang X, Liu F, Shi R, Yu C, Cao R. A reactive power sharing strategy of VSG based on virtual capacitor algorithm. IEEE Trans Ind Electron 2017;64(9):7520–31.
[29] Zhang B, Li D, Wang Y, Yan X. Self-adaptable reactive power-voltage controller for virtual synchronous generators. J Eng 2019;16:2969–73.
[30] Kundur P. Power system stability and control. EPRI power system engineering series. McGraw Hill; 1994.
[31] Yuan H, Yuan X, Hu J. Modeling of grid-connected VSCs for power system small-signal stability analysis in DC-link voltage control timescale. IEEE Trans Power Syst 2017;32(5):3981–91.
[32] Liu S, Xu Z, Hua W, Tang G, Xue Y. Electromechanical transient modeling of modular multilevel converter based multi-terminal HVDC systems. IEEE Trans Power Syst 2014;29(1):72–83.
[33] Venikov VA, Stroev VA, Idelchick VI, Tarasov VI. Estimation of electrical power system steady-state stability in load flow calculations. IEEE Trans Power Apparatus Syst 1975;94(3):1034–41.
[34] Model Library of PSS/E 33 [Z]. America: PTI Inc; 2013.